Supplemental Materials to a manuscript by Antonenko et al. "Derivatives of Rhodamine 19 as mild mitochondria-targeted cationic uncouplers"

Methods

FCS experimental setup. The home-made setup was described previously in (2). Briefly, fluorescence excitation and detection utilized a Nd:YAG solid state laser with a 532-nm beam attached to an Olympus IMT-2 epifluorescent inverted microscope equipped with a 40x, NA 1.2 water immersion objective (Carl Zeiss, Jena, Germany). The fluorescence passed through an appropriate dichroic beam splitter and a long-pass filter and was imaged onto a 50-μm core fiber optic coupled to an avalanche photodiode (SPCM-AQR-13-FC, Perkin Elmer Optoelectronics, Vaudreuil, Quebec, Canada). The signal from the output was sent to a personal computer using a fast interface card (Flex02-01D/C, Correlator.com, Bridgewater, NJ). The data acquisition time was 30 s. To calibrate the setup, we recorded the autocorrelation function of fluorescence of a solution of Rhodamine 6G, which was characterized by the correlation time τ_D estimated from equation (1). Assuming the diffusion coefficient of the dye to be 2.5 x 10^{-6} cm^2/s, the value of the confocal radius ω = 0.42 μm was obtained. The correlated fluorescence emission signals were fitted to the three-dimensional autocorrelation function (3).

$$G(\tau) = 1 + \frac{1}{N}\left(\frac{1}{1+\frac{\tau}{\tau_D}}\right)\left(\frac{1}{\sqrt{1+\frac{\omega^2\tau}{z_0^2\tau_D}}}\right) \qquad (1S)$$

with τ_D being the characteristic correlation time during which a molecule resides in the observation volume of radius ω and length z_0, given by $\tau_D = \omega^2/4D$, where D is the diffusion coefficient and N is the mean number of fluorescent particles in the confocal volume. In case of measurements of C_4R1 and C_4R4 at neutral and alkaline pH, equation 1S gave only a poor fit of these autocorrelation functions, which can be accounted for by a system heterogeneity characterized by the populations of monomers and aggregates. Equation 2S can be used to describe $G(\tau)$ in this case (4).

$$G(\tau) = \sum_{i=m,a} A_i g_i(\tau) \qquad (2S),$$

where $g_i(\tau)$ are autocorrelation functions of monomers ($g_m(\tau)$) and aggregates ($g_a(\tau)$), which can be described by equation 1, and A_m and A_a are their corresponding portions.

ATP synthesis. ATP synthesis was determined from a pH change measured with 30 μM Phenol Red (difference in absorption at 557 and 618 nm with an Aminco DW-2000 spectrophotometer) in the standard mixture comprised of 150 mM KCl, 0.5 mM EDTA, 5.5 mM $MgCl_2$, 5 mM KH_2PO_4, 0.5 mg/ml BSA, 2.5 mM HEPES(KOH), pH 7.4, according to (1). The sensitivity was calibrated by the addition of small aliquotes of titrated 20 mM HCl to the reaction mixture. After the addition of mitochondria (protein concentration, 0.4 mg/ml), 1 μM rotenone, 5 mM succinate, and 0.5 mM ADP were supplemented. Rhodamine derivatives were incubated with mitochondria for 5 min before the measurements.

Results

Effect of N-ethylmaleimide, aspartate, and Ruthenium Red on SkQR1-mediated respiration.

Figure 1S shows that the increase in the respiration rate caused by C_{12}R1 was insensitive to the addition of N-ethylmaleimide (panel A), glutamate (panel B), and Ruthenium Red (panel C).

pH dependence of aggregation of C_4R1 and C_4R4 in aqueous solution

To estimate the pK of rhodamine derivatives, we measured the pH dependence of self-aggregation of short-chain C_4R1 and C_4R4 by the FCS method. Autocorrelation functions (G(τ)) of SkQR1and SkQR4 showed that the compounds formed micelles or aggregates in the whole range of pH (data not shown), whereas C_4R1 and C_4R4 were monomers at pH = 4 and formed aggregates upon alkalinization (Fig. 2S). Figure 2S displays a series of autocorrelation functions of C_4R1 (panel A) and C_4R4 (panel B) taken at different pH values. The functions at pH 4 superimposed on that of rhodamine 6G (monomer standard) while they shifted to the right toward long times upon alkalinization, suggesting a decrease in the diffusion coefficient caused by aggregation. The degree of aggregation was substantially greater in the case of C_4R4 compared to C_4R1. The data were analyzed using equation 2 describing two-component diffusion of monomers and aggregates, and Fig. 2S (panel C) shows the pH dependence of a portion of the second component A_a, which can be approximated by a Henderson–Hasselbach curve with apparent pK = 7.3 (C_4R1) and pK = 5.3 (C_4R4).

Intracellular localization of C_{12}R1 and C_{12}R4

It has been shown previously that green fluorescent protein (GFP) fused with a mitochondria targeted sequence (mtGFP) can be used for visualization of mitochondria in yeast cells (6). Fig.3S, panel A shows the intracellular localization of C_{12}R1 and C_{12}R4. As expected, both compounds co-localize with mitochondria which fluoresced in green channel due to

expression of mtGFP. The addition of a protonophore FCCP prevented the accumulation of C_{12}R1 and C_{12}R4 in mitochondria (Fig. 3S, panel B).

Electron Microscopy of yeast cells in the presence of C_{12}R1 and C_{12}R4

We applied electron microscopy to monitor the effects of high concentrations of C_{12}R1 and C_{12}R4 on mitochondria in yeast cells. Representative microphotographs show that while high concentration of C_{12}R1 induces massive swelling and dramatic changes in mitochondrial ultrastructure, the changes caused by the same level of C_{12}R1 are much less pronounced (Fig. 4S). Table 1 shows the statistics of the appearance of swelling mitochondria. In the case of C_{12}R4 there were mitochondria partially swelled as well as having the area at least 10 times higher than the area occupied by the control mitochondria.

Molecular dynamics simulations.

Molecular dynamics approach was applied to simulate transmembrane movement of the SkQR1 and C_{12}-TPP^+ ions through BLM (movies 1 and 2). At the starting point of our simulations, we placed C_{12}TPP or SkQR1 ion in the polar part of DPPC lipid leaflet at one side of the membrane, and after 100 ns equilibration, the biasing potential (equation 2) was applied to C_{12}TPP or SkQR1 ions, respectively, starting form the ion equilibrium position z_0. Comparing motion of SkQR1 and C_{12}TPP in the bilayer in equilibrium, we observed that (i) SkQR1 was buried by ~0.2 nm deeper into the membrane, (ii) the π-conjugated aromatic ring of rhodamine lied parallel to the membrane surface, and (iii) the hydrocarbon linker in SkQR1 had a much higher freedom to adopt arbitrary conformation in the membrane, whereas the hydrocarbon tail of C_{12}TPP was strictly oriented along the normal to the membrane plan. The last two features apparently could be explained by different geometry of C_{12}TPP or SkQR1 ions: whereas the charged part of C_{12}-TPP^+ has an almost spherical shape with the effective size of less than 7 Å, the charged moiety of SkQR1 has a planner geometry with the dimension of about 10 Å, that stronger perturbs the lipid structure and creates some “free” space in the internal part of the membrane under the aromatic ring of rhodamine.

When the the biasing potential was applied, both ions started to bury into the membrane, and till the depth of ~0.5 nm from the membrane center, the behavior of both ions was similar. The quantitative difference between the ions was that in the case of SkQR1 the potential barrier increased more sharply than that in the case of C_{12}-TPP^+. In this region the orientation of the aromatic ring of rhodamine in SkQR1 remained parallel to the membrane surface. However, when the ions buried deeper into the membrane, the orientation of rhodamine ring changed form parallel to orthogonal relative the membrane surface. The change of rhodamine ring orientation

occurred gradually in the interval from +0.5 to -0.5 nm from the membrane center. Remarkably, in the middle of membrane the rhodamine ring spanned the nonpolar poration of the bilayer, so one of the nitrogen atom of rhodamine ring interacted with the water "finger" from the one side of the membrane, and the second nitrogen atom interacted with the symmetrical water "finger" at another side of the membrane. In the case of C_{12}TPP transfer, the change of ion orientations occurred much more sharply in the middle of bilayer, and because of the smaller size of ion, the conformation where C_{12}TPP spanned the narrow hydrophobic part between two large water-filled cavities at both sides of membrane was rather unstable. This explains the different potential barriers of 20 kJ/mol and 27 kJ/mol, calculated for C_{12}TPP and SkQR1, respectively. The profile of the free energy of SkQR1 and C_{12}TPP versus transmembrane distance is shown in Fig.5S. In agreement with this theoretical data, the translocation rate constant of C_{12}TPP was shown to be about one order of magnitude smaller than that of SkQR1 (8).

Mitochondrial ATP synthesis

Uncoupling effect implies stimulation of respiration accompanied by inhibition of phosphorylation. Both processes are related to a decrease in $\Delta\bar{\mu}_{H^+}$ which serves as a source of energy for conversion of ADP into H^+-ATP by ATP-synthase. Figure 6S shows the effect of SkQR1 and other compounds on ATP production by isolated rat liver mitochondria. As the formation of ATP from ADP and inorganic phosphate is accompanied by consumption of hydrogen ions, the rate of this reaction was determined from changes in absorption of the pH-sensitive probe phenol red (1). Control experiments showed that the addition of 1 μM oligomycin completely blocked the ATP synthesis (data not shown). As seen from Figure 6S, the ATP synthesis was inhibited not only by SkQR1, C_{12}R1, and FCCP, but also by C_{12}R4, although C_{12}R4 did not stimulate respiration. The effect of C_{12}R4 may result from direct inhibition of ATP-synthase by this lipophilic cation. In fact, it has previously been shown that micromolar concentrations of rhodamine 6G (C_2R1) and rhodamine 3B (C_2R4) inhibit ATP hydrolysis by isolated mitochondrial ATPase (5). Importantly, in our experiments the inhibiting concentrations of C_{12}R1 were higher than those of C_{12}R4, which in combination with the data on respiration and $\Delta\psi$ measurements suggests that C_{12}R1 and SkQR1 operated as true uncouplers in our system.

Reference List

1. Zharova, T. V. and Vinogradov, A. D. (2004) *J Biol.Chem* **279,** 12319-12324

2. Perevoshchikova, I. V., Zorov, D. B., and Antonenko, Y. N. (2008) *Biochim.Biophys.Acta* **1778,** 2182-2190

3. Krichevsky, O. and Bonnet, G. (2002) *Rep.Prog.Phys.* **65,** 251-297

4. Rusu, L., Gambhir, A., Mclaughlin, S., and Radler, J. (2004) *Biophys.J* **87,** 1044-1053

5. Mai, M. S. and Allison, W. S. (1983) *Arch.Biochem.Biophys* **221,** 467-476

6. Westermann, B. and Neupert, W. (2000) *Yeast* **16,** 1421-1427

7. Yang, H., Ren, Q., and Zhang, Z. (2006) *FEMS Yeast Res.* **6,** 1254-1263

8. Rokitskaya, T.I., Klishin, S.S., Severina, I.I., Skulachev, V.P. and Antonenko, Y.N. (2008) *Biochim.Biophys.Acta* **224**, 9-19

Legends to Figures

Fig. 1S. The increase in the respiration rate of mitochondria caused by $C_{12}R1$ was insensitive to the addition of N-ethylmaleimide (50 μM, panel A), glutamate (2 mM, panel B), and Ruthenium Red (4 μM, panel C). Conditions are the same as in Fig.2 of the main text except for the experiment shown in panel B which was carried out in the medium containing 250 мM sucrose, 0.5 мM EGTA, 5 mM MOPS, 3 mM $MgCl_2$, 3 mM KH_2PO_4, pH 7.0**.**

Fig. 2S. A and B. Normalized autocorrelation functions of 10 nM C_4R1 (panel A) and C_4R4 (panel B) at different pH (black curves) and corresponding approximations with equation 2 (gray curves). **C.** pH dependence of a portion of the second component A_a of equation 2 fitted by a Henderson–Hasselbach curve with pK = 7.3 (C_4R1) and pK = 5.3 (C_4R4).

Fig.3S. Mitochondrial localization of $C_{12}R1$ and $C_{12}R4$ depends on the membrane potential. ***A***, $C_{12}R1$ (25 nM) and $C_{12}R4$ (250 nM) co-localize with mitochondria-targeted green fluorescent protein (mtGFP). ***B***, FCCP inhibits mitochondrial accumulation of $C_{12}R1$ and $C_{12}R4$. 5 μM FCCP was added prior to $C_{12}R1$ (50 nM) or $C_{12}R4$ (250 nM). Fluorescence filers used: λexcitation = 470-495 nm, λsplit =505 nm, λemission = 510-550 nm (UMNIBA3 filter set, imaging of GFP), and λexcitation = 530-550 nm, λsplit =570 nm, λemission = 590 nm (U-MNG2 filter set, imaging of $C_{12}R1$ and $C_{12}R4$). Incubation time with $C_{12}R1$ and $C_{12}R4$ was 10 minutes. Bar, 5 μm. For colocalization analysis of mtGFP with C12R1 or C12R4 the cells were transformed with pYX223 plasmid pretreated with Nhe1 restriction enzyme. This plasmid encodes GFP fused to mitochondrial targeting sequence (6).

Fig.4S. $C_{12}R4$ but not $C_{12}R1$ induces dramatic swelling of mitochondria in yeast cells shown by electron microscopy.

a, control cells. Mitochondria shown by black arrows

b, cells treated with $C_{12}R1$ (10 μM) contain normal-looking (black arrows) and slightly swollen (white arrows) mitochondria

c and *d*, cells treated with $C_{12}R4$ (10 μM) contain slightly and heavily swollen mitochondria (white arrows) with abnormal cristae.

Bar, 5 μm. Electron microscopy was done as in (7).

Fig.5S. Potential of Mean Force (PMF) for penetration of cations SkQR1 (A) and C_{12}TPP (B) through the lipid membrane in umbrella sampling molecular dynamics. The PMFs were calculated by Eqn. (1) using the biasing potential (2) for the trajectories shown in Movie 1 and 2, respectively.

Fig. 6S. Dose dependence of the effect of SkQR1, C_{12}R1, C_{12}R4, and FCCP on the ATP synthesis. The synthesis of ATP by rat liver mitochondria was measured by the pH probe phenol red as described above. In all experiments, 5 mM of succinate and 2 μM of rotenone were used to start the process.

Table 1. Quantification of changes in mitochondrial ultrastructure induced by C_{12}R1 and C_{12}R4. Representative mitochondria are shown in Supplementary Fig. 4 and indicated by arrows. The values correspond to the percentage of cells containing at least one swollen mitochondria of either type.

Sample/percentage of cells containing particular type of mitochondria	Slightly swollen / with clarified matrix	Heavily swollen: the area occupied is at least 10 times higher than the area occupied by the control mitochondria	Number of cells analyzed
Control	0	0	156
C_{12}R1, 10 μM	28	0	265
C_{12}R4, 10 μM	15	45	238

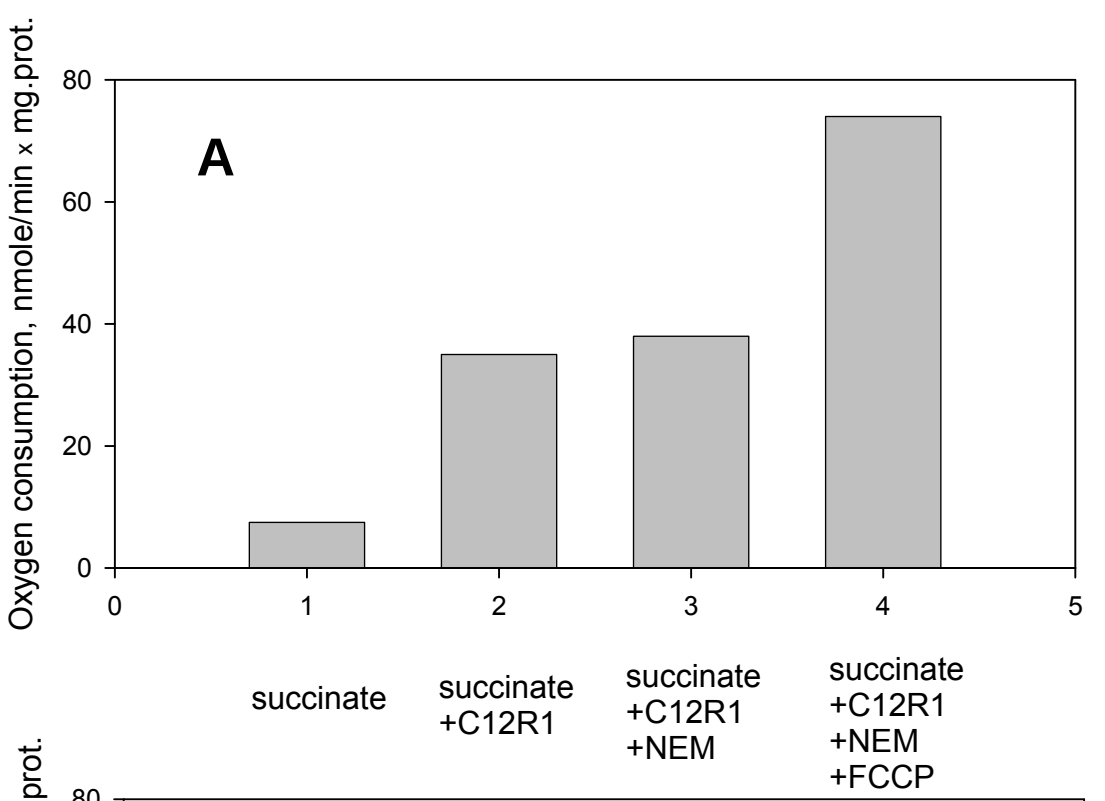

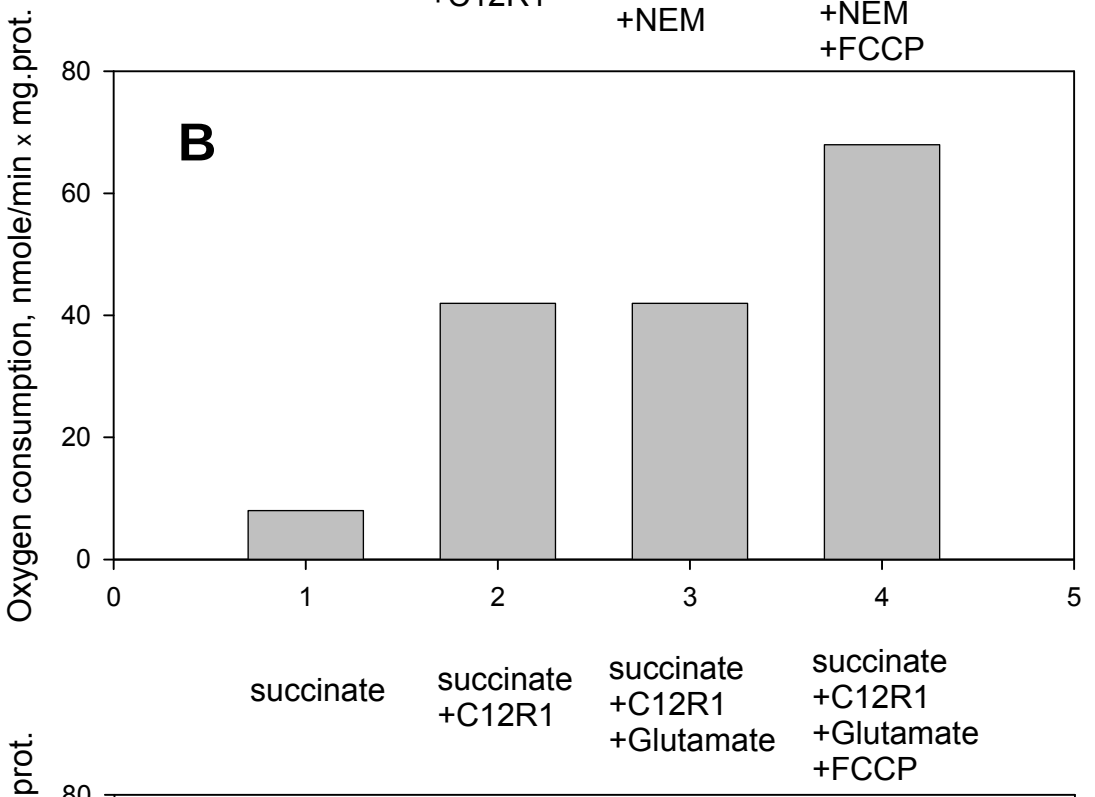

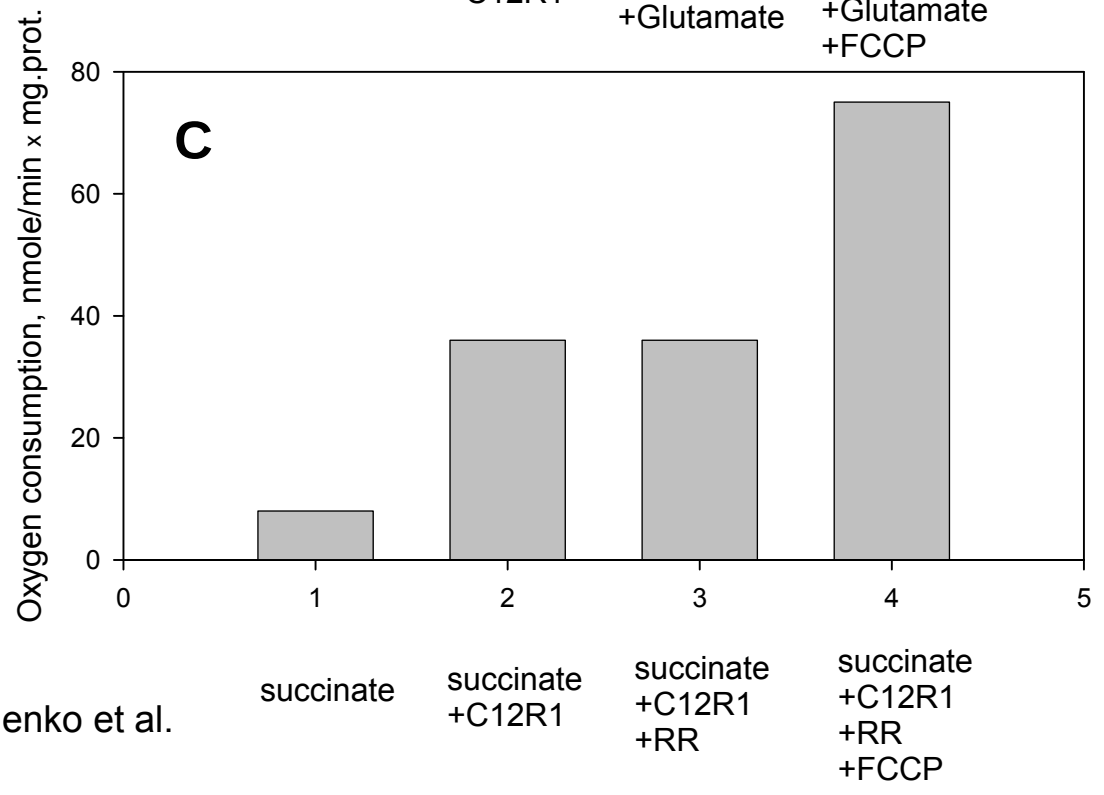

Fig.1S, Antonenko et al.

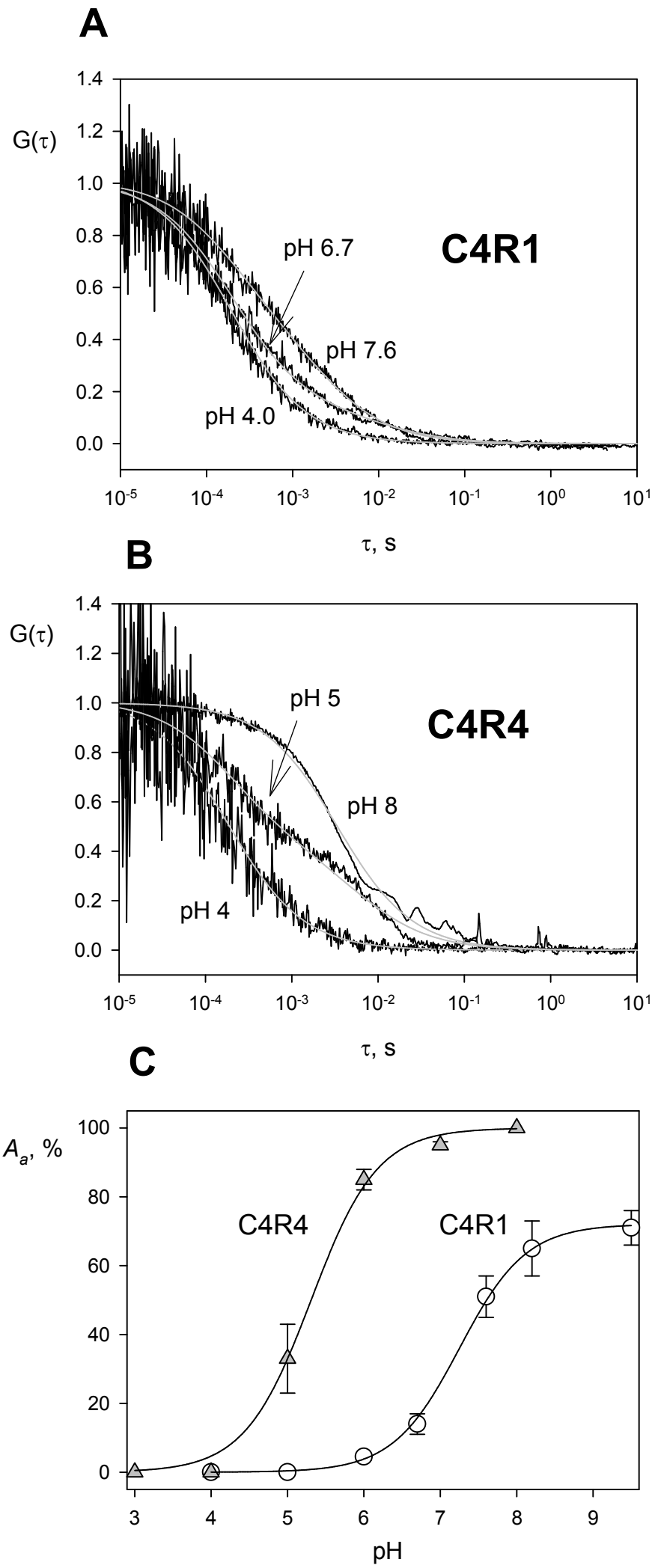

Fig.2S, Antonenko et al.

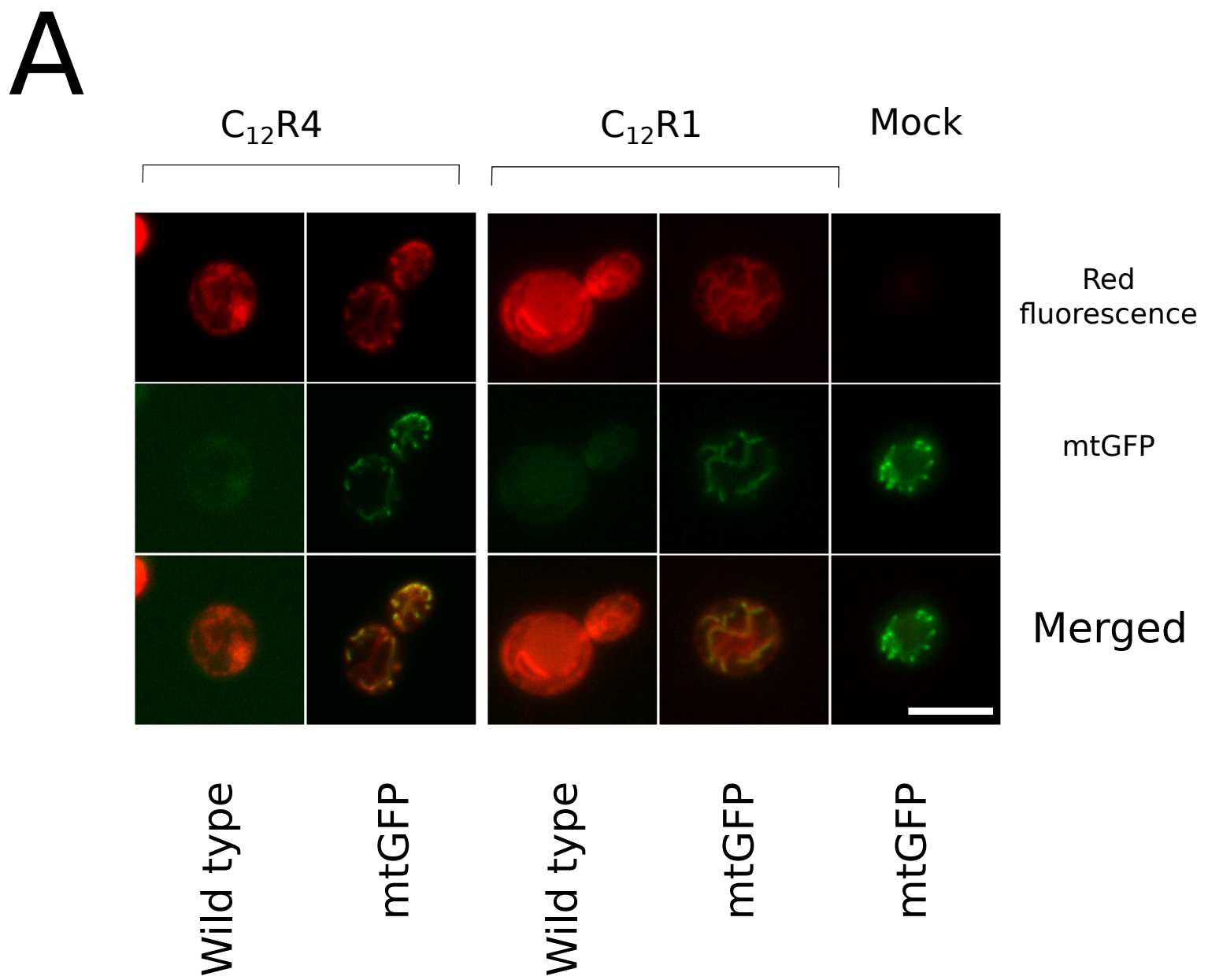

Fig.3S, Antonenko et al.


a

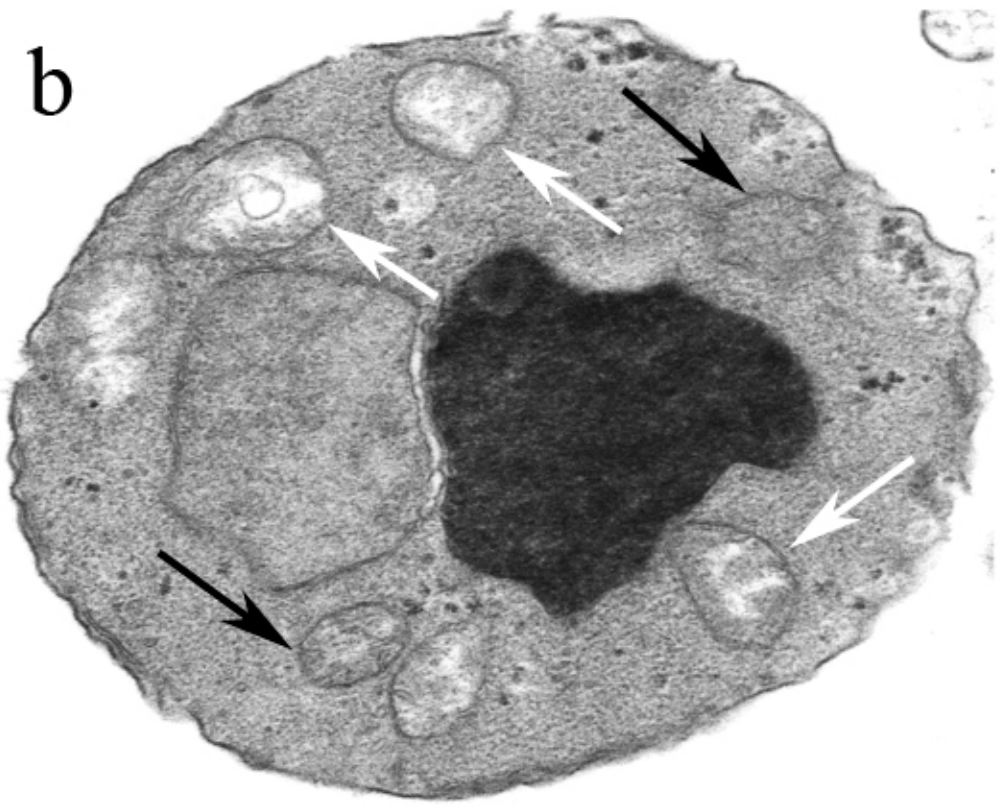
b

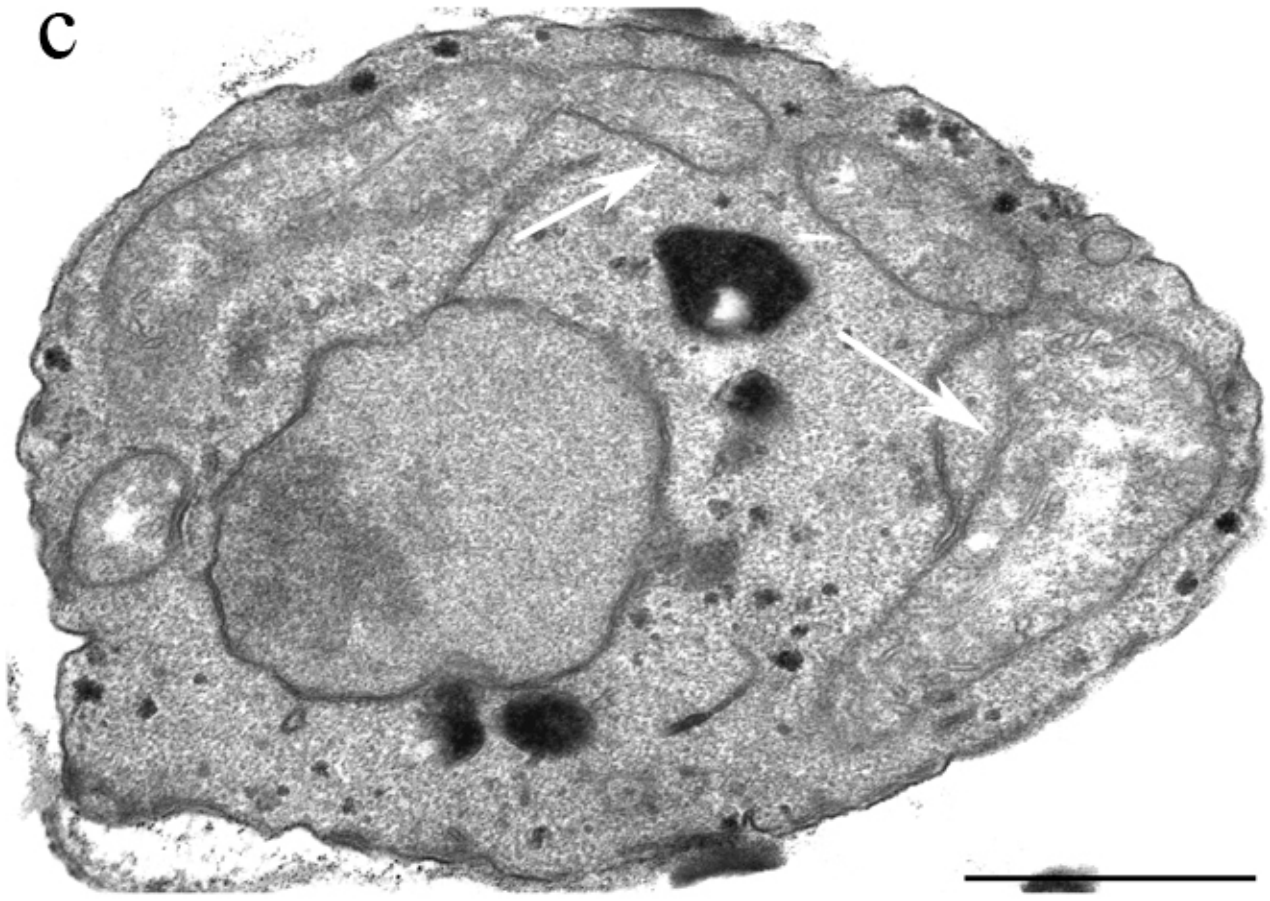
c


d

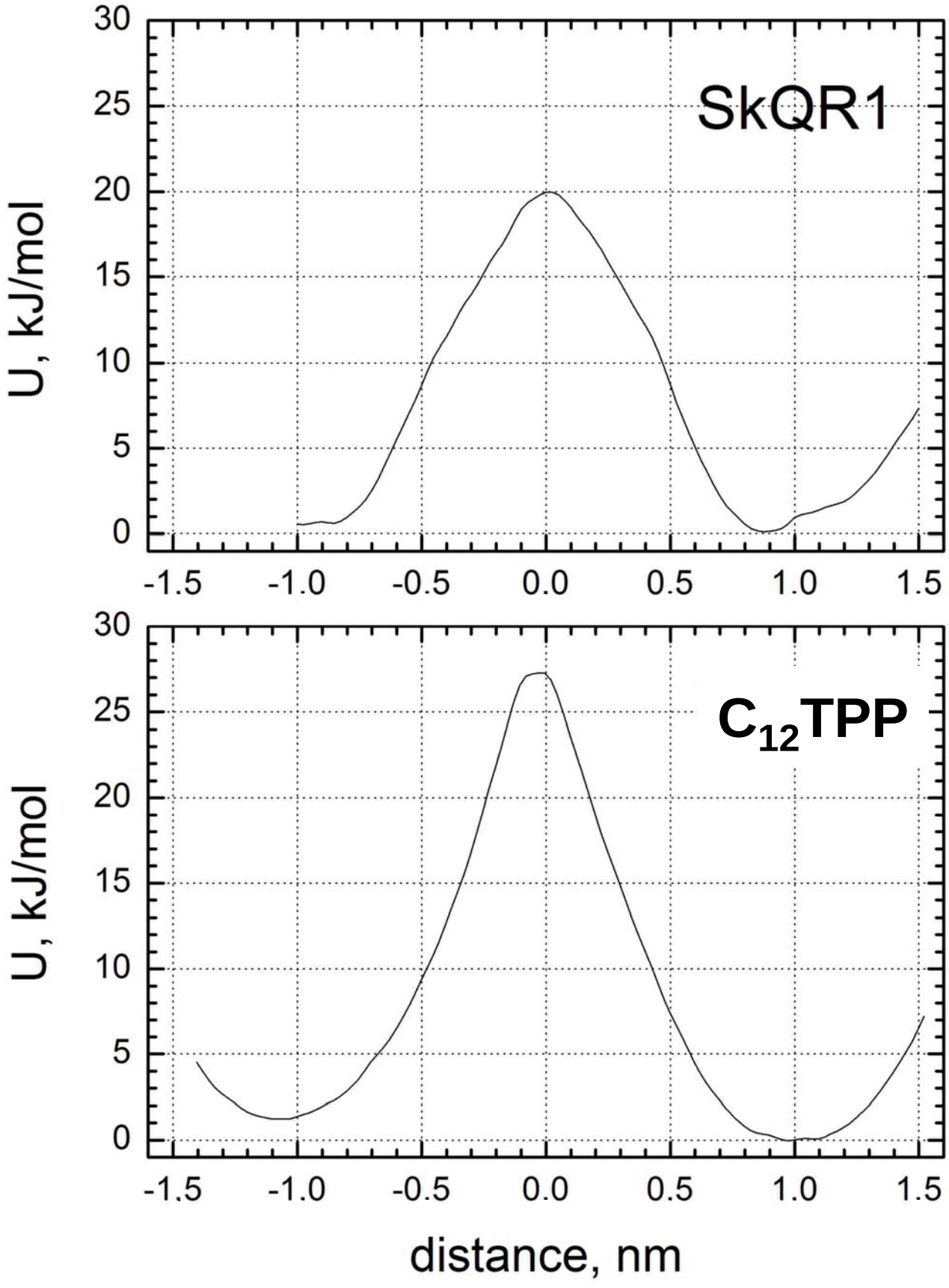

Fig.5S, Antonenko et al.

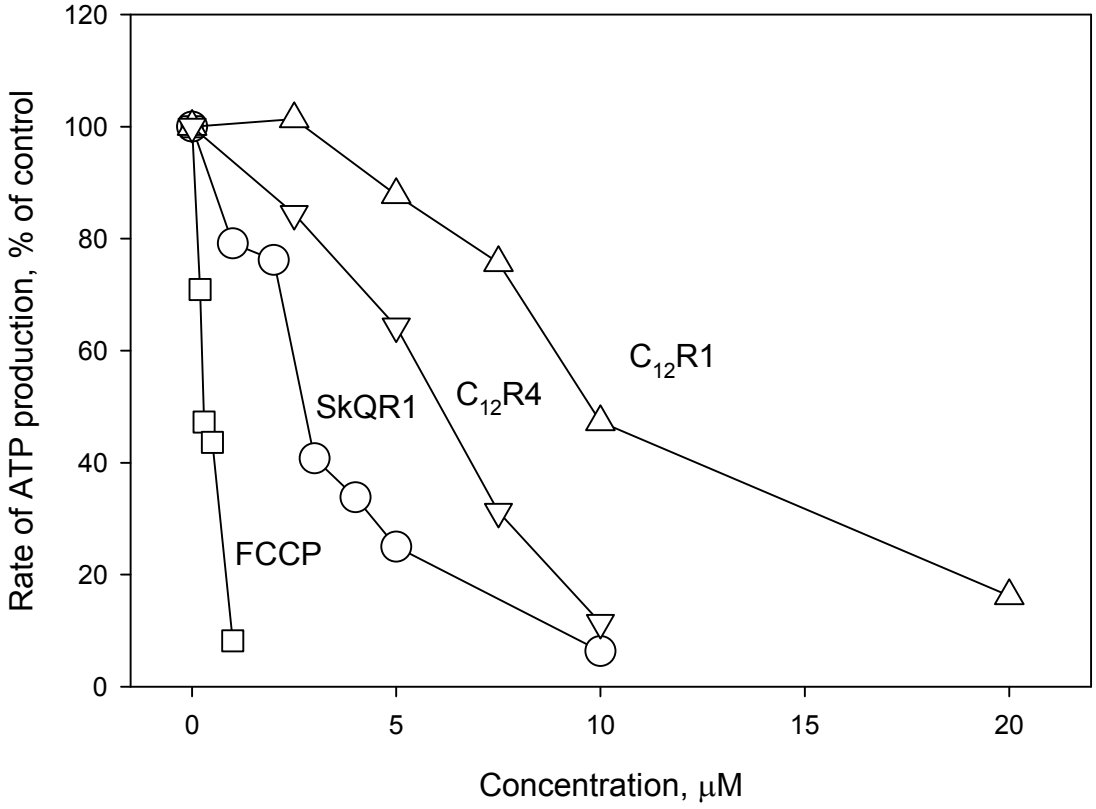

Fig.6S, Antonenko et al.